THE JOURNAL OF PHYSICAL CHEMISTRY C

Article

pubs.acs.org/JPCC

Electrochemical Characterization and Quantified Surface Termination Obtained by Low Energy Ion Scattering and X-ray Photoelectron Spectroscopy of Orthorhombic and Rhombohedral $LaMnO_3$ Powders

Emmanouil Symianakis,[†] Daniel Malko,[†] Ehsan Ahmad,[†,‡] Anne-Sophie Mamede,[§] Jean-Francois Paul,[§] Nicholas Harrison,[†,‡] and Anthony Kucernak*[,†]

[†]Department of Chemistry and [‡]Thomas Young Centre, Imperial College London, South Kensington, London SW7 2AZ, U.K.

[§]Unité de Catalyse et de Chimie du Solide, UMR CNRS 8181, Université Lille 1, Cité Scientifique, Bâtiment C3, 59655 Villeneuve d'Ascq Cedex, France

Supporting Information

ABSTRACT: $LaMnO_3$ powder synthesized by glycine combustion synthesis with the rhombohedral and orthorhombic structures has been characterized by the combination of low energy ion scattering (LEIS) and X-ray photoelectron spectroscopy (XPS), while the electrocatalytic activity for the oxygen reduction reaction is measured with the rotating disk electrode (RDE) method. Quantification of the surface terminations obtained by LEIS suggests that the orthorhombic $LaMnO_3$ crystallites are near thermodynamic equilibrium as surface atomic ratios compare well with those of equilibrium morphologies computed by a Wulff construction based on computed surface energies. Both rhombohedral and orthorhombic structures present the same La/Mn atomic ratio on the surface. Electrochemical activity of the two structures is found to be the same within the error bar of our measurements. This result is in disagreement with results previously reported on the activity of the two structures obtained by the coprecipitation method [Suntivich et al. *Nat. Chem.* **2011**, *3* (7), 546], and it indicates that the preparation method and the resulting surface termination might play a crucial role for the activity of perovskite catalysts.

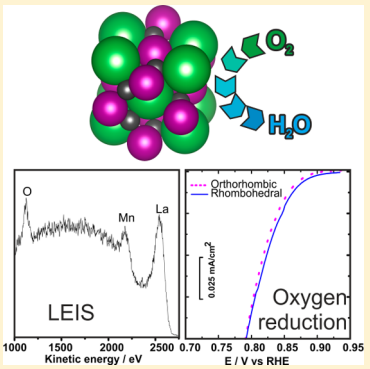

INTRODUCTION

$LaMnO_3$ is an ABO_3 perovskite with a known catalytically active surface and applications in solid oxide fuel cells (SOFCs)[2] and alkaline fuel cells (AFCs).[3] At room temperature $LaMnO_3$ adopts the rhombohedral structure. Annealing of rhombohedral $LaMnO_{3+\delta}$ at 1173 K and cooling to room temperature under N_2 environment results in the formation of orthorhombic stoichiometric $LaMnO_3$ as shown by means of neutron and X-ray powder diffraction (XRD).[4,5] Using electron paramagnetic resonance, it has been possible to correlate the influence of oxygen stoichiometry to the catalytic activity of $LaMnO_3$,[6] while density functional theory (DFT) calculations suggest that the active site for the oxygen reduction reaction (ORR) is the on-top position of the surface Mn ions.[7−10] Based on this hypothesis Suntivich et al.[1] explained the higher electrochemical activity of the rhombohedral structure, compared to that of the orthorhombic, by correlating the ORR activity for oxide catalysts primarily to the s*-orbital (e_g) occupation and the covalency of the B-site transition-metal−oxygen interaction. Although it is accepted that this type of ORR activity identifiers obtainable by DFT calculations can enhance the predictive ability of theoretical calculations for the engineering of new nonprecious ORR catalysts, it is the detailed experimental characterization of the first atomic layer of the samples as synthesized that will allow the reliable correlation of such theoretical predictions to the observed electrocatalytic activities. Recently, we have postulated that strong electron correlation is found to play an important role in determining the nature of the reaction sites. By including on site electronic correlation in DFT calculations, it was determined that symmetry-breaking Jahn−Teller distortions lead to six distinct surface sites, only one of which is found to bind O_2 with an intermediate binding energy while facilitating the formation of the superoxide O^{2-} that is necessary for the ORR to proceed.[11]

The surface of $LaMnO_3$ oxides obtained by a variety of synthetic methods have been characterized by X-ray photoelectron spectroscopy (XPS) before,[12−16] while low energy ion scattering (LEIS) has also been used for the characterization manganites[17] and other perovskite oxides.[18]

In this paper we report the first, to our knowledge, quantified characterization of the surface termination obtained from $LaMnO_3$ powders synthesized via glycine combustion with the

Received: March 21, 2015
Revised: May 11, 2015
Published: May 12, 2015

DOI: 10.1021/acs.jpcc.5b02742
J. Phys. Chem. C 2015, 119, 12209−12217

rhombohedral and orthorhombic structures by the combination of LEIS and XPS, while electrochemical characterization is performed by the rotating disk electrode (RDE) method. Furthermore, the elemental composition of the first atomic layer obtained by LEIS from the orthorhombic phase presents the La/Mn atomic ratio that would be expected from thermodynamically equilibrated crystallites as predicted by Wulff construction predictions of crystallite morphology based on DFT surface energies.[10]

EXPERIMENTAL SECTION

In order to avoid quantification errors due to strong neutralization matrix effects that have been reported between certain metals and their various oxidized states,[19,20] La_2O_3 and Mn_2O_3 powder reference samples with 99.99% purity were purchased from Sigma-Aldrich[21] and used for the determination of the La/Mn sensitivity factor that we used for the quantification of our LEIS results. The Mn_2O_3, La_2O_3, and both $LaMnO_3$ powders were hand pressed into pellets and introduced into the ultra high vacuum (UHV) chamber. The as-received Mn_2O_3 powder was characterized by XPS and showed no contaminations, with a detection limit of 0.1% atomic concentration, whereas LEIS that is sensitive to the outermost atomic layer revealed contamination by Na. In order to remove Na from the Mn_2O_3 powder, it was rinsed in a Soxhlet extractor for 14 days prior to pellet formation. This method led to the reduction of the Na signal below the detection limit of the LEIS instrument, 1−0.05% of a monolayer for light elements like Na. XPS analysis revealed that the La_2O_3 powder had a surplus of nonstoichiometric oxygen. The removal of the adsorbed oxygen species from the La_2O_3 powder was achieved by annealing at 1000 °C for 5 h in an air atmosphere prior to introduction to the UHV chamber[13] and confirmed by XPS. The LEIS spectra obtained from the reference oxides are presented in Figure 5.

$LaMnO_3$ powders were prepared by glycine combustion synthesis. Before use La_2O_3 was calcined at 1000 °C in order to remove water. To a mixture of La_2O_3 (3.0 g, 9.2 mmol, 99.9% Sigma-Aldrich) and Mn powder (1.0 g, 18.4 mmol, >99.9% Sigma-Aldrich), nitric acid (68%, 6.6 mL, BDH) was slowly added. The nitrate ions serve as oxidant during the combustion process. Glycine was then added (8.16 g, 116 mmol, >99% Sigma-Aldrich), which acts as the fuel in the combustion process. To the slurry was added deionized water (2 mL, 18.2 MΩ) in order to obtain a solution and facilitate uniform distribution of the reactants. The solution was heated to 80 °C on a hot plate for 3 h to remove excess water. A gel was formed which was then heated to 300 °C in order to facilitate autoignition and combustion of the material. The resulting brown fluffy solid was placed into a tube furnace and heated to 450 °C at a rate of 5 °C/min, under a constant stream of air, and held there for 2 h. This ensured that the combustion reaction was completed before the temperature was further raised. Subsequently the temperature was raised to 1000 °C at a rate of 2 °C/min and held there for 12 h. After cooling and analysis it was found that the resulting material is the rhombohedral or oxygen-rich phase $LaMnO_3$-rhombohedral. Part of the material was then placed in the tube furnace again and heated to 600 °C at a rate of 2 °C/min under a nitrogen atmosphere and held there for 12 h, in order to transform it into the orthorhombic or oxygen-deficient phase $LaMnO_3$-orthorhombic as characterized by XRD.[4,5]

The LEIS technique is described elsewhere.[22,23] LEIS experiments were performed in a Qtac[100] instrument (ION-TOF GmbH) at a base pressure of 3×10^{-10} mbar (which increases to the 10^{-8} mbar range during the analysis due to the flux of noble gas). The instrument is described elsewhere.[21,23] The samples were analyzed using a 3 keV He^+ primary ion beam directed perpendicularly to the target surface at an analyzer pass energy of 3 keV. The area of analysis is 1 mm × 1 mm, and the experiments have been performed with two settings initially with total dose per spectrum of 3.5×10^{14} ions/cm^2 and in some cases repeated for confirmation using new $LaMnO_3$ pellets with total dose per spectrum of 1.9×10^{14} ions/cm^2, while typically the beam current was set to 5 nA. Quantification of the peaks were carried out using XPSPEAK41 software. Quantification is performed using linear background subtraction.

X-ray photoelectron spectroscopy (XPS) analyses were performed using a Kratos Analytical AXIS Ultra^{DLD} spectrometer. A monochromatic aluminum source (Al Kα = 1486.6 eV) was used for excitation. The analyzer was operated in constant pass energy of 40 eV using an analysis area of approximately 700 μm × 300 μm. Charge compensation was applied to minimize charging effects occurring during the analysis. The adventitious C 1s (285.0 eV) binding energy (BE) was used as internal reference. Pressure was in the 10^{-10} mbar range during the experiments. Quantification and simulation of the experimental photopeaks were carried out using CasaXPS and XPSPEAK41 software. Quantification is performed using nonlinear Shirley background subtraction. XPS spectra obtained from the orthorhombic phase are presented in the Supporting Information, Figures ESI.14−ESI.19.

The XPS and LEIS instruments along with the atomic oxygen source are connected by a radial chamber at a pressure of 3×10^{-9} mbar, which allowed the transfer of the samples from one instrument to the other without exposure to air.

The LEIS relative sensitivity factors for La and Mn were evaluated from the prepared La_2O_3 and Mn_2O_3 powders. The LEIS intensity ratio based on the areas of the La and Mn peaks as obtained from the Mn_2O_3 and La_2O_3 powders by 3 keV He^+ kinetic energy and 3 keV pass energy is La/Mn = 0.92.

XRD was performed using a PANalytical X'Pert Pro XRD system with a Cu anode (Kα = 8048.0 eV) operated at 40 kV with a current of 120 mA which confirmed the rhombohedral and orthorhombic structures for both of the synthesized batches.

The oxygen reduction reaction (ORR) activity of the materials was assessed with the rotating disk electrode (RDE) method. In order to increase the conductivity of the catalyst layer, the catalyst ink was prepared by a mixture of $LaMnO_3$ to carbon with Ketjen Black EC600 (Akzo Nobel), at a 5:1 ratio, similar to a procedure described in the literature.[24] The Ketjen Black (KB) was treated in hydrochloric acid at 80 °C overnight in order to remove metal impurities. It was then filtered and washed with deionized water (Milli-Q 18.2 MΩ) and dried in an oven at 120 °C before use. Na^+ exchanged Nafion solution was prepared as per the literature.[24] The inks were ultrasonicated with the appropriate amount of Na^+ exchanged Nafion solution and THF (>99.9% Sigma-Aldrich) for 1 h before use. The final concentration of the ink was 5 mg_{oxide} mL^{-1}_{ink}, 1 mg_{KB} mL^{-1}_{ink}, and 1 mg_{Nafion} mL^{-1}_{ink}. For the electrode preparation, 10 μL of ink was drop-casted onto a glassy carbon disk electrode (Pine Instruments LLC, USA, 0.196 cm^2) which was mirror polished with an alumina slurry

DOI: 10.1021/acs.jpcc.5b02742
J. Phys. Chem. C 2015, 119, 12209−12217

(0.05 μM, Buehler) prior to use.[24] The cast film was then dried under a constant rotation at 400 rpm. This has shown to yield highly uniform catalyst layers. The catalyst layer which was always examined with a magnifying glass looked uniform and flat throughout all experiments.

Electrochemical characterizations were conducted in a three compartment electrochemical glass cell. The RDE was connected to a rotator (Pine, AFMSRCE). The reversible hydrogen reference electrode (RHE, Gaskatel, HydroFlex) was ionically connected to the main compartment of the electrochemical glass cell via a Luggin–Haber capillary. A glassy carbon rod was used as the counter electrode. Glassy carbon was used instead of Pt in order to avoid contamination with catalytically active precious metals. The potential was controlled with a Metrohm Autolab PGStat. The 0.1 M NaOH electrolyte was prepared from NaOH pellets (ACS Reagent grade, Sigma-Aldrich). In order to minimize silicate dissolution from the glass into the electrolyte and possible poisoning of the catalyst,[1,24,25] a freshly prepared electrolyte solution was used prior to every measurement. Tests involving doping the electrolyte with controlled amounts of silicate indicate that there should be no degradation due to contamination effects in these experiments (Supporting Information). For cleaning, the electrochemical cell was first placed into a solution of acidified $KMnO_4$ (ACS Reagent grade, Sigma-Aldrich) for 24 h, then rinsed thoroughly with deionized water, and then placed into a solution consisting of 1:1 H_2SO_4:2% H_2O_2 for 24 h. The cell was then again soaked in deionized water multiple times and thoroughly rinsed with deionized water before use. This ensured that no organic contaminants or trace metals were present during the measurement. All measurements were conducted at 10 mV s^{-1} in either N_2 or O_2 (BIP ultrahigh purity grade, Air Products) at room temperature and atmospheric pressure. A measuring protocol described in the literature was followed.[1,24] In short ORR activities were obtained from the negative-going scans in pure O_2 saturated solutions at 1600 rpm and were corrected for capacitive currents in pure N_2. Error bars represent standard deviations from at least three independent repeated measurements. "Independent" here means that the same batch of material was used, but the measurements were carried out from different inks and with fresh electrolytes with cleaning of the glass cell in between as described above. The potential range was kept within 0.7–1 V vs RHE to prevent degradation of the catalyst.[24]

RESULTS AND DISCUSSION

XPS Characterization of $LaMnO_3$ Powder As Synthesized. XPS spectra of the La 3d, Mn 2p, O 1s, and C 1s regions were obtained from the rhombohedral $LaMnO_3$ powder as synthesized. Elemental quantification with XPS results give 19.2% La, 15.9% Mn, 50.9% O, and 14.0% C atomic concentrations, leading to a La/Mn atomic ratio of 1.2, in good agreement with the literature.[12] After charge correction the binding energy of La $3d_{5/2}$ is found to be 834.3 ± 0.1 eV. Figure 1 shows the O 1s region that is obtained from the rhombohedral $LaMnO_3$ sample as received. It presents a peak at P1 = 529.8 ± 0.1 eV which is attributed to lattice oxygen, a peak at P2 = 531.0 ± 0.1 eV attributed to adsorbed O_2^{2-}/O^- possibly related to carbonate species present, and finally a peak at P3 = 532.0 ± 0.1 eV which is attributed to hydroxyl groups and/or adsorbed oxygen species.[14,15]

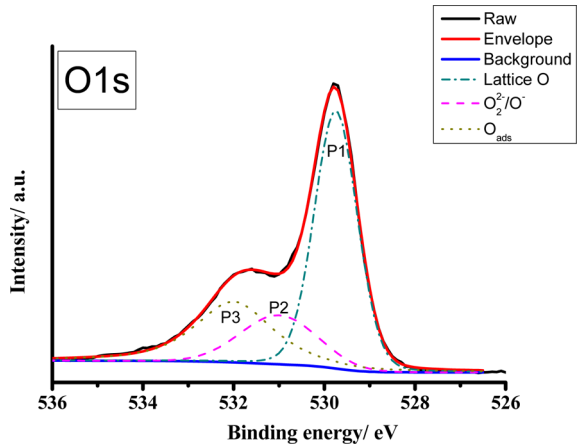

Figure 1. XPS spectrum and peak deconvolution of O 1s region of the rhombohedral $LaMnO_3$ sample.

Figure 2 shows the XPS spectrum for the Mn 2p region. The position of the raw Mn $2p_{3/2}$ peak is observed at 642.1 ± 0.1 eV,[15] while deconvolution based on reference spectra obtained from Mn_2O_3 and MnO_2 powder samples with raw positions of the peaks at 642.1 ± 0.1 and 642.8 ± 0.1 eV respectively[26] suggests a ratio of Mn^{4+}/Mn^{3+} = 0.3. This decomposition, leading to the majority presence of Mn^{3+}, is confirmed by the calculation of an average oxidation state of Mn of around 3.3 thanks to the use of the doublet separation of Mn 3s[12,27] presented in the Supporting Information, Figures ESI.11 and ESI.19, for the rhombohedral and orthorhombic phases, respectively.

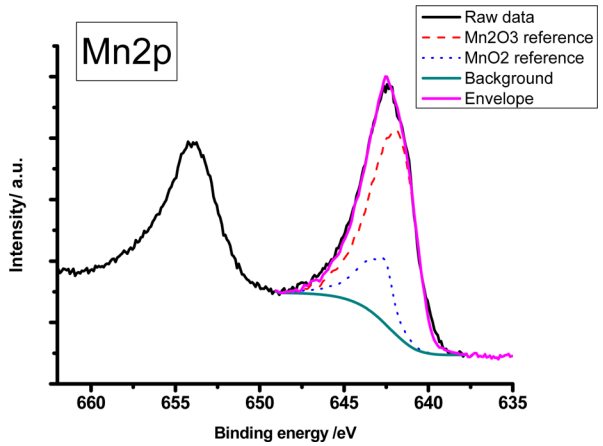

Figure 2. XPS spectrum and peak deconvolution of the Mn 2p region of the rhombohedral $LaMnO_3$ sample based on reference spectra obtained from Mn_2O_3 and MnO_2 samples. The ratio of Mn^{4+}/Mn^{3+} species is estimated to be 0.3.

In the case of C 1s and La 4s region, Figure 3, the position of the La 4s peak is at 274.7 eV while the C 1s main peak, which is attributed to adventitious carbon, is set to 285.0 eV and is used as a reference for the correction of spectra against charging effects. A second peak appears at 289.2 ± 0.1 eV which is attributed to surface carbonates. Finally, a third peak at 286.3 ± 0.1 eV is attributed to C–O bonds.[28]

Preparation of the Pristine Surfaces. In order to remove the carbon present at the surface, observed by XPS and confirmed by LEIS, the pellets are exposed to an atomic oxygen

DOI: 10.1021/acs.jpcc.5b02742
J. Phys. Chem. C 2015, 119, 12209–12217

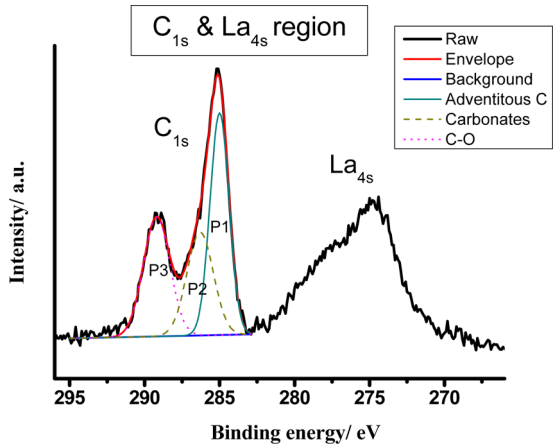

Figure 3. XPS spectrum and peak deconvolution of the La 4s and C 1s region of the rhombohedral $LaMnO_3$ sample.

source in the UHV chamber. After 1 h of exposure the XPS C 1s signal is no longer observed.

LEIS spectra after the removal of carbon suggested that residual atomic oxygen remained on the surface of the powder and influenced the absolute and relative intensities of La and Mn ions.

In order to remove the residual atomic oxygen, two strategies were implemented. The first was to anneal the samples, in this case a pellet of rhombohedral $LaMnO_3$, at temperatures up to 350 °C and up to 1 h, in order to desorb the remaining oxygen. The second was to obtain a large number of LEIS spectra thus performing sputtering with the He^+ beam until the relative and absolute intensities of La and Mn remained unaffected. This usually occurred after a total He ion dose of about 2.0×10^{15} ions/cm^2. For reference, a single measurement applies a dose of either 3.5×10^{14} or 1.9×10^{14} ions/cm^2.

This steady state does not necessarily mean that the adsorbed atomic oxygen is completely removed from the surface but rather that a certain number of Mn sites might more easily lose their adsorbed oxygen atoms than others, which results in a steady state of the measured La/Mn ratio determined by the sputtering conditions used and the UHV environment.

This interpretation is supported by theoretical calculations, which predict that the Mn−O_4 octahedron sites of the surface will bind the atomic oxygen considerably stronger than the rest of the Mn adsorption sites,[11] which should result in an up to 20% increase of the measurable La/Mn atomic ratio.

Annealing Experiments Characterized by LEIS and XPS. LEIS spectra obtained from both orthorhombic and rhombohedral $LaMnO_3$ powders both before and after exposure to the atomic oxygen source were recorded. Furthermore, in the case of the rhombohedral $LaMnO_3$, the sample was annealed within the UHV chamber and exposed to atomic oxygen until the carbon signal was reduced below the detection limit of LEIS.

Annealing to temperatures up to 350 °C alone was unsuccessful in revealing the pristine surface as it resulted in segregation of further carbon from the bulk of the material to its outermost surface. This led to complete coverage of the surface as was evidenced by LEIS, but it offered a method for the evaluation of the effectiveness of the atomic oxygen source used in this experiment.

XPS spectra of the C 1s region obtained after annealing at high temperatures are deconvoluted as described above and are consistent with a model in which at least two layers of different carbon species form upon annealing. The first one consists of carbonates covering the surface while the second layer, above the carbonates, consists of sp^3 C bulk carbon. There may be a third layer composed of carbon bonded to oxygen. However, this species may alternatively exist in the second layer as a mixture with the bulk carbon. This carbon is probably remnants of glycine or its decomposition products from the synthetic route that was followed.

The C 1s (carbonate)/La 4s intensity ratio is consistently found to be the same regardless of the annealing temperature and time. This result suggests that carbon forms a single atomic layer over the pristine $LaMnO_3$ surface while the rest of the segregating carbon builds upon that initial layer as sp^3 C.

The relative sensitivity factors provided by Kratos Analytical for C 1s and La 4s are 0.278 and 0.192, respectively. The La relative sensitivity factor has been corrected for its presence in the $LaMnO_3$ to 0.106.[29] Based on the predictions of a layered model which takes into account the deconvoluted intensities of C 1s (carbonates) and La 4s, and assuming the surface of the $LaMnO_3$ is initially completely covered by a single layer of carbonate with a thickness of 0.278 nm,[30] we can estimate an inelastic mean free path (IMFP) value for the photoelectrons of La 4s and C 1s to be around 1.5 nm.[31]

The same model reproduces the experimental intensity ratio of C 1s (carbonate)/La 4s, after annealing at 350 °C for 1 h, when it is assumed that complete carbonate coverage occurs. Spectra obtained after exposure of the annealed sample to the atomic oxygen source for 10 and 20 min are reproduced if it is assumed that 50 ± 5 and 20 ± 5% respectively of the surface is covered by carbonate.

When the IMFP values obtained from the database provided by NIST[32,33] for La 4s and C 1s of 2.9 nm are used, the calculated thickness after annealing is estimated to be 0.53 nm—roughly two monolayers of carbonate. In this case the experimental C 1s (carbonate)/La 4s intensities obtained after 10 and 20 min of exposure to atomic oxygen are also reproduced by the model when ∼50 and ∼20% of the surface is covered with carbonate.

The differences arising from the two initial assumptions used in the model result mainly from the surface roughness of the sample and the actual atomic relative sensitivities of carbon compared to the value used due to the complexity of the carbon−oxide interface which includes C−Mn, C−La, and C−O bonds.

However, in both cases the models predict ∼50 and ∼20% of the surface to be free after the application of oxygen when we assume that annealing results in a single atomic layer of carbonate on the surface. This agreement can occur only when the coverage under study is under one atomic layer and the intensity of the covering layer depends directly on the percentage of the free surface. Furthermore, the alternative prediction of the second model where a complete layer of carbonate could be covering the surface after exposure of the sample to atomic oxygen for 10 min can be dismissed based on the strong La and Mn direct backscattering signals and the increase of the LEIS absolute intensities of La and Mn signals which support the interpretation of 50 and 20% of the surface being uncovered.

Following annealing at 350 °C and exposure of the pellet to the atomic oxygen source for 10 min, the carbon signal is

DOI: 10.1021/acs.jpcc.5b02742
J. Phys. Chem. C 2015, 119, 12209−12217

reduced to below the detection limit of LEIS following sample transfer to the XPS instrument via the radial chamber at 10^{-9} mbar pressure. XPS in this case suggests that about 50% of the surface is free of carbon contamination as discussed above.

Although ~50% of the $LaMnO_3$ surface is still covered by three layers of carbon species, $LaMnO_3$/carbonate/adventitious carbon/C−O, the low work function of the adventitious carbon in combination with the oxygen covering the carbon at the top layer results in poor detectability of the remaining carbon contamination by LEIS under the measurement conditions.[34]

A second exposure to the atomic oxygen source for another 10 min was performed, and 80% of the surface is found to be carbon free according to XPS while LEIS presented a small increase of ~20% in the absolute intensities of the La and Mn peaks. The evolution of the C 1s and O 1s spectra during exposure to the atomic oxygen source is presented in the Supporting Information, Figures ESI.12 and ESI.13.

LEIS Characterization of $LaMnO_3$ Pristine Surfaces. Two fresh pellets of rhombohedral and orthorhombic $LaMnO_3$ powders from the first batch were exposed to the atomic oxygen source for 10 min after introduction into the UHV chamber. The steady state spectra obtained by LEIS are presented in Figure 4, where the La/Mn intensity ratios for the rhombohedral and orthorhombic powders used in this experiment are determined to be 2.9 ± 0.4 and 2.8 ± 0.4, respectively. An additional 10 min of exposure to the atomic oxygen source results in a small increase of the La and Mn absolute intensities by ~20% with a La/Mn intensity ratio of 3.3 ± 0.4 achieved after reaching steady state following He^+ sputtering (Figure 5a). Nevertheless, the La/Mn intensity ratio is slightly affected, leading to a change comparable to the error of the measurement obtained with 50% carbon coverage (Figure 4).

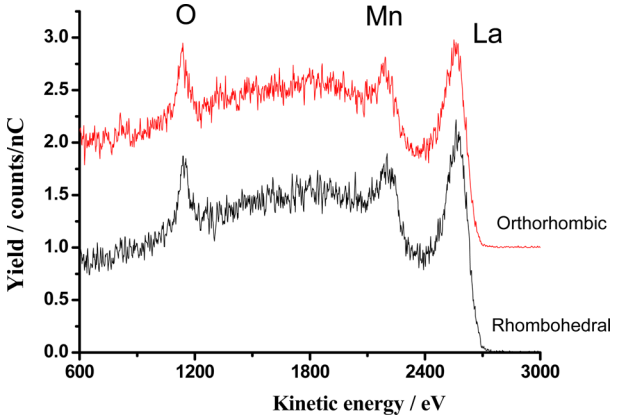

Figure 4. LEIS spectra for rhombohedral and orthorhombic $LaMnO_3$ powders after exposure to the atomic oxygen source for 10 min.

Quantification of the Surface Atomic Concentrations by LEIS. The yield of ions, S_i, backscattered from a surface atom of mass m_i, is a measure for the atomic surface concentration N_i according to[21]

$$S_i = \frac{I_p}{e} t \xi R n_i N_i \tag{1}$$

where I_p is the primary ion beam current and e is the elementary charge; t is the acquisition time; ξ is an instrumental factor including detector efficiency, solid angle, and analyzer transmission; R is a factor which takes into account the surface roughness and the shielding by neighboring atoms; and, finally, n_i is the elemental sensitivity factor, given by

$$n_i = P_i^+ \frac{d\sigma_i}{d\Omega} \tag{2}$$

with the ion fraction

$$P_i^+ = S_i^+/(S_i^+ + S_i^0) \tag{3}$$

in which S^+ is the signal of scattered ions and S^0 is the signal of backscattered neutrals.

Since the spectra are obtained with the same instrumental conditions I_p, t, ξ, and $d\sigma_i/d\Omega$ are constants. Furthermore, the pellets are hand pressed while the specific surface areas of the powders used are 2.96 and 0.09 $m^2\ g^{-1}$ for La_2O_3 and Mn_2O_3 respectively as measured by the Brunauer−Emmett−Teller (BET) method. This specific surface area range is expected to impose a decrease of the measured intensity of less than 20% when compared to flat surface samples.[35] This error range is within the overall error of these measurements.

Relative sensitivity factors can be obtained in this case based on calibration against these reference powder samples if their

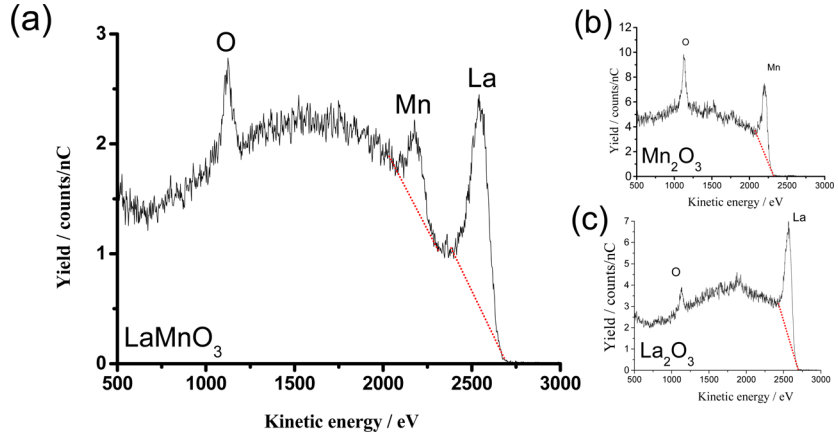

Figure 5. (a) LEIS spectrum from the orthorhombic $LaMnO_3$ powder after exposure to atomic oxygen source for 20 min and steady state is achieved due to He^+ sputtering during collection of the spectrum. Spectra from the reference materials, (b) Mn_2O_3 and (c) La_2O_3, used for calculation of the La/Mn relative sensitivity factor. The dotted lines signify the linear background used.

DOI: 10.1021/acs.jpcc.5b02742
J. Phys. Chem. C 2015, 119, 12209−12217

atomic surface concentration can be estimated and with the assumption that there are no significant matrix effects associated with the different oxides so that P_i^+ remains the same.[21,35−37]

In order to estimate the atomic surface concentrations N_{La}^{ref} and N_{Mn}^{ref} of La and Mn in their respective oxides, we assume that atomic surface concentration is equal to $(\rho_i^*)^{2/3}$ with $\rho_i^* = \rho_i N_A/M_i$, where N_A is 6.02×10^{23} atoms/mol, ρ_i is the bulk density (in g cm^{-3}), and M_i is the atomic mass (in g mol^{-1}) of element i.[36]

Based on these assumptions we obtain atomic surface concentrations of 1.0×10^{15} and 2.2×10^{15} atoms cm^{-2} for La and Mn from their reference oxides, respectively. Since the La/Mn intensity ratio obtained by LEIS, with 3 keV $^4He^+$ and pass energy of 3 keV, from the two oxides is 0.92, the cationic relative sensitivity factor with those operating conditions is calculated within an error of ∼20% to be 1.92.

When we apply this to the La/Mn intensity ratio obtained for the rhombohedral and orthorhombic $LaMnO_3$, we find La/Mn atomic ratios of 1.5 and 1.7, respectively. These values differ by ∼10% and are the same within the total error bar.

Comparison of the La/Mn Atomic Ratio to Wulff Construction Predictions. DFT calculations of the surfaces on the orthorhombic phase carried out in previous work indicate a similar ratio[10] to result from the terminating surfaces of an equilibrated crystal as predicted by the Wulff construction of equilibrium crystallite morphology, where the detection of ions at the surface is predicted based on the line of sight of the incident He ions, taking into account the ionic radii of the La^{3+}, Mn^{3+}, and O^{2-}. Notably, it is observed that 60% of the surface is constituted of stoichiometric O, 28% is La, and 12% is Mn while it is predicted that the measurable La/Mn ratio should vary from 1.4, to 1.8 depending on whether the Mn from the exposed Mn−O_4 octahedron at the surface is considered to be detected, or inhibited by the strong adsorption of O, which is indicated in recent DFT calculations.[11] The excellent agreement of the measured La/Mn atomic ratio to the values expected from the thermodynamically equilibrated system suggests that the $LaMnO_3$ powder with the orthorhombic phase as synthesized is near thermodynamic equilibrium.

Atomic Oxygen Adsorption and Low Dose He^+ Ion Sputtering Experiment. Although the pristine surface of the $LaMnO_3$ powder is obtained by exposure of the powder to the atomic oxygen source, a process that removes surface carbon, it is observed that application of the atomic oxygen source on the pristine surface has a measurable effect by itself.

Upon exposure of the surface to atomic oxygen even for very short periods of time, the signal characteristic of direct backscattering from the Mn atoms is removed from the spectra. Consecutive low ion doses of He^+ (∼1.8×10^{14} ions cm^{-2} for each spectrum—about 0.1 monolayer) eventually restore the Mn intensity to the initial value, after exposure to a total dose of around 2.1×10^{15} ions cm^{-2}. This is a fully reversible and reproducible effect occurring on the pristine surfaces of both rhombohedral and orthorhombic structures suggesting that oxygen atoms have been adsorbed on top of the Mn atoms effectively shadowing them as evidenced by the first spectrum. For comparison, sputtering of the $LaMnO_3$ surface atoms is expected to be around 1−2% for this dose of He^+.[35]

Exposure of the surface to atomic oxygen also results in a decrease of the La intensity, but the shape of the direct backscattering peak is not affected. This decrease of La intensity after the exposure to the atomic oxygen source is attributed to an increased Auger neutralization, an effect with nonlocal character, imposed by the oxygen adsorbed over the Mn atoms leading to an increased density of electrons at the surface.[38] Removal of the weakly adsorbed oxygen atoms by low ion dose, effectively nondestructive ion sputtering, reveals the shadowed Mn atoms and reduces the Auger neutralization of the La and O atoms comprising the surface, allowing them to obtain their full measurable intensity, as shown in Figure 6. Due to this

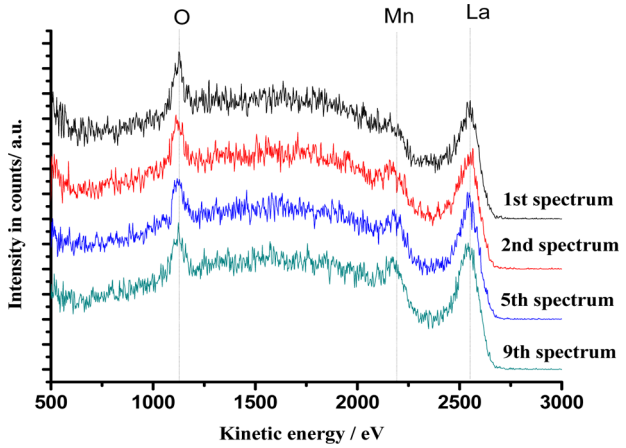

Figure 6. Orthorhombic $LaMnO_3$ after exposure to atomic oxygen source for 10 min. Each spectrum corresponds to a total dose of 3.5×10^{14} ions/cm^2. Although the first scan suggests only traces of Mn atoms on the first atomic layer, the second presents a clear contribution, while several consecutive scans slowly increase the Mn and La intensities toward steady state values after exposure of the surface to a total dose of 2.1×10^{15} ions/cm^2.

increase of the substrate oxygen intensity, the oxygen peak remains unaffected by the loss of around 12% of adsorbed oxygen covering the Mn atoms. This result provides direct experimental confirmation that atomic oxygen adsorbs on top of the Mn atoms as has been predicted by theoretical calculations[1,8−10] and supports the idea that the catalytically active site is the position on top of manganese as has been proposed.

Electrochemical Characterization. Characterization of the catalytic activity of the as prepared $LaMnO_3$ powders from both batches that were synthesized are presented in Figure 7 as normalized current densities for the measured catalysts. Normalization was performed with respect to the surface area determined with the BET method (see Supporting Information). The potentials measured at a specific current density of 25 μA cm^{-2} are as follows: rhombohedral 840 (±28) mV (RHE), orthorhombic 818 (±19) mV(RHE) from the first batch, and rhombohedral 819 (±15) mV(RHE), orthorhombic 813 (±12) mV(RHE), from the second. The difference in the activity measured between the rhombohedral and orthorhombic powders lies within the standard deviation for our measurements and does not allow the conclusion of a significantly higher activity of the rhombohedral or oxygen-rich phase as described in the literature.[1] All values fall within the value reported for the orthorhombic phase of 834 (±24) mV versus RHE.[1] Figure 8 shows the potential at 25 μA cm^{-2} and the respective standard deviation. This indicates that the preparation method and the surface termination might play a crucial role for the activity of perovskite catalysts. Our catalyst was prepared by the glycine combustion method as opposed to

DOI: 10.1021/acs.jpcc.5b02742
J. Phys. Chem. C 2015, 119, 12209−12217

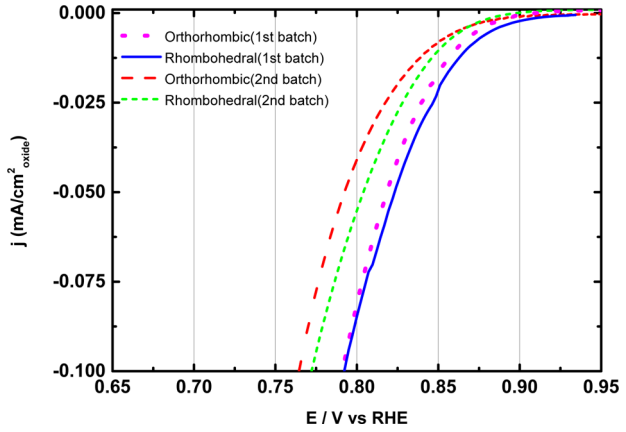

Figure 7. RDE cyclic voltammetry of $LaMnO_3$-orthorhombic and $LaMnO_3$-rhombohedral, obtained from both batches with1600 rpm in O_2-saturated 0.1 M NaOH. Scan rate, 10 mV/s; loading, 250 $\mu g_{oxide}/cm^2$, 50 $\mu g_{carbon}/cm^2$, 50 $\mu g_{Nafion}/cm^2$. Current normalized to specific surface area of the perovskite.

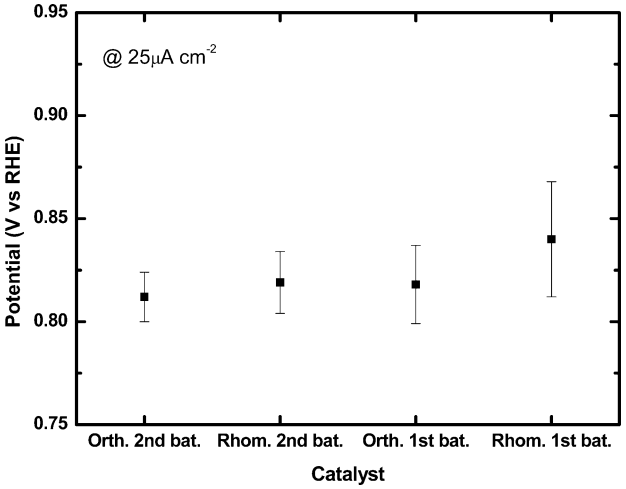

Figure 8. Potentials at 25 $\mu A/cm^2$ $LaMnO_3$-orthorhombic and $LaMnO_3$-rhombohedral, obtained from both batches. Error bars represent standard deviation of at least three independent measurements.

the one in the literature, which was prepared by the coprecipitation method.[1]

In order to exclude possible effects of known contaminants that might inhibit the rhombohedral catalyst compared to the literature value, poisoning experiments were performed. Chloride was added, because the carbon used to increase the electrical conductivity of the catalyst layer was treated with HCl and it is likely that a certain amount of chloride will not be removed by the filtration and washing steps performed. Moreover, chloride is a known contaminant for Pt based catalysts under acidic conditions.[39] However, no significant effect is visible (Supporting Information). It has been shown that contaminants which are leached from glass in alkaline solutions can impact the performance of Pt based catalysts;[25] therefore, $NaSiO_3$ was added to the solution in order to exclude this possibility. At a concentration of 10^{-3} M, which is approximately 2 orders of magnitude larger than the concentration of silicate expected after a short exposure to an alkaline electrolyte,[25] a minute decrease in performance is visible. Higher concentrations of 10^{-2} and 10^{-1} M lower the performance further, but if silicate was a strong poison which even acts at the concentrations reported,[25] the impact is expected to be significantly larger at those concentrations. Hence this possibility can also be excluded. Additional to the small effect of the silicate, it is not expected that other contaminants that might have leached into the solution from the glass play a significant role, as the electrolyte was each time freshly prepared and the measurements carried out quickly without a prolonged exposure to the electrolyte solution. However, in order to totally exclude this possibility, the experiment should be repeated in a ptfe cell.[25] Meticulous care was taken throughout all experiments, to avoid any other contaminations. The large scatter found might be due to the complex nature of the ink and effects of inhomogeneous mixing.

CONCLUSION

The surface termination of the first atomic layer of $LaMnO_3$ powder synthesized by glycine combustion synthesis with the rhombohedral and orthorhombic structures has been characterized by LEIS for the first time. XPS spectra suggest that the initially synthesized rhombohedral powder is similar to the $LaMnO_3$ powder synthesized by Nuns et al.[12] XRD confirms the different $LaMnO_3$ structures. LEIS results after quantification suggest that the La/Mn surface atomic ratios of the two phases are 1.5 and 1.7 $\pm$ 0.3. Furthermore, the La/Mn atomic ratio measured is in excellent agreement with the range of values predicted from the Wulff construction of crystallite morphology for the orthorhombic phase when we assume that the $Mn-O_4$ octahedron adsorbs the atomic oxygen too strongly to be effectively removed by He^+ sputtering with the conditions applied, with 1.4 for a perfectly clean surface and up to 1.8 for completely covered $Mn-O_4$ octahedron sites. Furthermore, the low dose sputtering experiment, using the He^+ primary beam of the LEIS instrument, after exposure of the samples to an atomic oxygen source provides direct experimental confirmation of the theoretical prediction that the atomic oxygen will preferentially adsorb on top of the Mn cations of the $LaMnO_3$ surface. Finally, the electrochemical activity of both phases is measured with the rotating disk electrode, but the performed measurements do not allow the observation of a significantly higher activity of the rhombohedral or oxygen-rich phase as previously reported.[1]

This indicates that the preparation method and the resulting surface termination might play a crucial role for the activity of perovskite catalysts since our catalyst was prepared by the glycine combustion method as opposed to the coprecipitation method used.[1]

ASSOCIATED CONTENT

Supporting Information

X-ray powder diffraction and SEM images of the $LaMnO_3$ used. Further XPS and LEIS spectra of samples and details of BET measurements on the powders. Further discussion of the electrochemical results including measurements of sensitivity of materials to contamination during the electrochemical measurements. The Supporting Information is available free of charge on the ACS Publications website at DOI: 10.1021/acs.jpcc.5b02742.

AUTHOR INFORMATION

Corresponding Author

*E-mail: anthony@imperial.ac.uk.

DOI: 10.1021/acs.jpcc.5b02742
J. Phys. Chem. C 2015, 119, 12209−12217

Notes

The authors declare no competing financial interest.

■ ACKNOWLEDGMENTS

The authors would like to acknowledge funding from the Engineering and Physical Sciences Research Council under Grants EP/G06704X/1 and EP/J016454/1.

■ REFERENCES

(1) Suntivich, J.; Gasteiger, H. A.; Yabuuchi, N.; Nakanishi, H.; Goodenough, J. B.; Shao-Horn, Y. Design principles for oxygen-reduction activity on perovskite oxide catalysts for fuel cells and metal-air batteries. *Nat. Chem.* **2011**, *3* (7), 546−550.

(2) Tao, S.; Irvine, J. T. S.; Kilner, J. A. An efficient solid oxide fuel cell based upon single-phase perovskites. *Adv. Mater.* **2005**, *17* (14), 1734.

(3) Hayashi, M.; Uemura, H.; Shimanoe, K.; Miura, N.; Yamazoe, N. Reverse micelle assisted dispersion of lanthanum Manganite on carbon support for oxygen reduction cathode. *J. Electrochem. Soc.* **2004**, *151* (1), A158−A163.

(4) Norby, P.; Andersen, I. G. K.; Andersen, E. K.; Andersen, N. H. The crystal structure of Lanthanum Manganate(III), $LaMnO_3$, at room temperature and at 1273 K under N_2. *J. Solid State Chem.* **1995**, *119* (1), 191−196.

(5) Rodriguez-Carvajal, J.; Hennion, M.; Moussa, F.; Moudden, A. H.; Pinsard, L.; Revcolevschi, A. Neutron-diffraction study of the Jahn-Teller transition in stoichiometric LaMnO3. *Phys. Rev. B* **1998**, *57* (6), R3189−R3192.

(6) Oliva, C.; Forni, L. EPR and XRD as probes for activity and durability of LaMnO3 perovskite-like catalysts. *Catal. Commun.* **2000**, *1*, 5−8.

(7) Wang, Y.; Cheng, H.-P. Oxygen Reduction Activity on Perovskite Oxide Surfaces: A Comparative First-Principles Study of LaMnO3, LaFeO3, and LaCrO3. *J. Phys. Chem. C* **2013**, *117* (5), 2106−2112.

(8) Pilania, G.; Ramprasad, R. Adsorption of atomic oxygen on cubic PbTiO3 and LaMnO3 (001) surfaces: A density functional theory study. *Surf. Sci.* **2010**, *604* (21−22), 1889−1893.

(9) Kotomin, E. A.; Mastrikov, Y. A.; Heifetsa, E.; Maier, J. Adsorption of atomic and molecular oxygen on the LaMnO(3)(001) surface: ab initio supercell calculations and thermodynamics. *Phys. Chem. Chem. Phys.* **2008**, *10* (31), 4644−4649.

(10) Ahmad, E. A.; Mallia, G.; Kramer, D.; Kucernak, A. R.; Harrison, N. M. The stability of LaMnO3 surfaces: a hybrid exchange density functional theory study of an alkaline fuel cell catalyst. *J. Mater. Chem. A* **2013**, *1* (37), 11152−11162.

(11) Ahmad, E. A.; Tileli, V.; Kramer, D.; Mallia, G.; Stoerzinger, K. A.; Shao-Horn, Y.; Kucernak, A. R.; Harrison, N. M. Optimising Oxygen Reduction Catalyst Morphologies from First Principles. In preparation.

(12) Nuns, N.; Beaurain, A.; Dinh, M. T. N.; Vandenbroucke, A.; De Geyter, N.; Morent, R.; Leys, C.; Giraudon, J. M.; Lamonier, J. F. A combined ToF-SIMS and XPS study for the elucidation of the role of water in the performances of a Post-Plasma Process using LaMnO3+delta as catalyst in the total oxidation of trichloroethylene. *Appl. Surf. Sci.* **2014**, *320*, 154−160.

(13) Sunding, M. F.; Hadidi, K.; Diplas, S.; Lovvik, O. M.; Norby, T. E.; Gunnaes, A. E. XPS characterisation of in situ treated lanthanum oxide and hydroxide using tailored charge referencing and peak fitting procedures. *J. Electron Spectrosc. Relat. Phenom.* **2011**, *184* (7), 399−409.

(14) Sun, M.; Zou, G.; Xu, S.; Wang, X. Synthesis of alumina supported LaMnO3 with excellent thermal stability by a PVP-assisted route. *Mater. Chem. Phys.* **2012**, *134* (1), 309−316.

(15) Hammami, R.; Aissa, S. B.; Batis, H. Effects of thermal treatment on physico-chemical and catalytic properties of lanthanum Manganite LaMnO3+y. *Appl. Catal., A* **2009**, *353* (2), 145−153.

(16) Ponce, S.; Pena, M. A.; Fierro, J. L. G. Surface properties and catalytic performance in methane combustion of Sr-substituted lanthanum manganites. *Appl. Catal., B* **2000**, *24* (3−4), 193−205. Srinivas, B.; Rao, V. R. S. XPS characterization of Gamma ray induced chemisorption of oxygen in Lanthanum Manganate ($LaMnO_3$). *J. Radioanal. Nucl. Chem.* **1995**, *191* (1), 35−44. Zampieri, G.; Abbate, M.; Prado, F.; Caneiro, A.; Morikawa, E. XPS and XAS spectra of CaMnO3 and LaMnO3. *Physica B: Condens. Matter* **2002**, *320* (1−4), 51−55.

(17) Poggini, L.; Ninova, S.; Graziosi, P.; Mannini, M.; Lanzilotto, V.; Cortigiani, B.; Malavolti, L.; Borgatti, F.; Bardi, U.; Totti, F.; Bergenti, I.; Dediu, V. A.; Sessoli, R. A Combined Ion Scattering, Photoemission, and DFT Investigation on the Termination Layer of a La0.7Sr0.3MnO3 Spin Injecting Electrode. *J. Phys. Chem. C* **2014**, *118* (25), 13631−13637.

(18) Druce, J.; Ishihara, T.; Kilner, J. Surface composition of perovskite-type materials studied by Low Energy Ion Scattering (LEIS). *Solid State Ionics* **2014**, *262*, 893−896.

(19) Vari, G.; Ovari, L.; Kiss, J.; Konya, Z. LEIS and XPS investigation into the growth of cerium and cerium dioxide on Cu(111). *Phys. Chem. Chem. Phys.* **2015**, *17* (7), 5124−5132.

(20) Napetschnig, E.; Schmid, M.; Varga, P. Growth of Ce on Rh(111). *Surf. Sci.* **2004**, *556* (1), 1−10.

(21) Brongersma, H. H.; Draxler, M.; de Ridder, M.; Bauer, P. Surface composition analysis by low-energy ion scattering. *Surf. Sci. Rep.* **2007**, *62* (3), 63−109.

(22) Brongersma, H. H.; Grehl, T.; Schofield, E. R.; Smith, R. A. P.; ter Veen, H. R. J. Analysis of the Outer Surface of Platinum-Gold Catalysts by Low-Energy Ion Scattering Improved resolution allows selective analysis of mixed metal systems. *Platinum Met. Rev.* **2010**, *54* (2), 81−87. Brongersma, H. H.; Grehl, T.; van Hal, P. A.; Kuijpers, N. C. W.; Mathijssen, S. G. J.; Schofield, E. R.; Smith, R. A. P.; ter Veen, H. R. J. High-sensitivity and high-resolution low-energy ion scattering. *Vacuum* **2010**, *84* (8), 1005−1007.

(23) Tellez, H.; Chater, R. J.; Fearn, S.; Symianakis, E.; Brongersma, H. H.; Kilner, J. A. Determination of O-16 and O-18 sensitivity factors and charge-exchange processes in low-energy ion scattering. *Appl. Phys. Lett.* **2012**, *101*, 15.

(24) Suntivich, J.; Gasteiger, H. A.; Yabuuchi, N.; Shao-Horn, Y. Electrocatalytic Measurement Methodology of Oxide Catalysts Using a Thin-Film Rotating Disk Electrode. *J. Electrochem. Soc.* **2010**, *157* (8), B1263−B1268.

(25) Mayrhofer, K. J. J.; Crampton, A. S.; Wiberg, G. K. H.; Arenz, M. Analysis of the impact of individual glass constituents on electrocatalysis on pt electrodes in alkaline solution. *J. Electrochem. Soc.* **2008**, *155* (6), P78−P81. Mayrhofer, K. J. J.; Wiberg, G. K. H.; Arenz, M. Impact of glass corrosion on the electrocatalysis on Pt electrodes in alkaline electrolyte. *J. Electrochem. Soc.* **2008**, *155* (1), P1−P5.

(26) Biesinger, M. C.; Payne, B. P.; Grosvenor, A. P.; Lau, L. W. M.; Gerson, A. R.; Smart, R. S. C. Resolving surface chemical states in XPS analysis of first row transition metals, oxides and hydroxides: Cr, Mn, Fe, Co and Ni. *Appl. Surf. Sci.* **2011**, *257* (7), 2717−2730.

(27) Galakhov, V. R.; Demeter, M.; Bartkowski, S.; Neumann, M.; Ovechkina, N. A.; Kurmaev, E. Z.; Logachevskaya, N. I.; Mukovskii, Y. M.; Mitchell, J.; Ederer, D. L. Mn 3s exchange splitting in mixed-valence manganites. *Phys. Rev. B* **2002**, *65*, 11.

(28) Ghodbane, S.; Ballutaud, D.; Deneuville, A.; Baron, C. Influence of boron concentration on the XPS spectra of the (100) surface of homoepitaxial boron-doped diamond films. *Phys. Status Solidi A* **2006**, *203* (12), 3147−3151.

(29) Seah, M. P. Quantitative AES and XPS: convergence between theory and experimental databases. *J. Electron Spectrosc. Relat. Phenom.* **1999**, *100*, 55−73.

(30) Jun, Y.-S.; Ghose, S. K.; Trainor, T. P.; Eng, P. J.; Martin, S. T. Structure of the hydrated $(10\bar{1}4)$ surface of rhodochrosite ($MnCO_3$). *Environ. Sci. Technol.* **2007**, *41* (11), 3918−3925.

(31) Symianakis, E.; Eyangelakis, G. A.; Ladas, S. On the origin of the substrate-induced oxidation of Ni/NiO(001) studied by X-ray Photoelectron Spectroscopy and Molecular Dynamics Simulations.

DOI: 10.1021/acs.jpcc.5b02742
J. Phys. Chem. C 2015, 119, 12209−12217

Surf. Sci. **2010**, *604* (11−12), 943−950. *Practical Surface Analysis*; Briggs, D., Seah, M. P., Eds.; Wiley: Chichester, U.K., 1990; Vol. *1*.
(32) National Institute of Standards and Technology. Electron Inelastic-Mean-Free-Path Database, version 1.1. http://www.nist.gov/srd/nist71.cfm.
(33) Dahle, S.; Voigts, F.; Maus-Friedrichs, W. In situ preparation of calcium carbonate films. *Thin Solid Films* **2012**, *520* (6), 1842−1846.
(34) Mikhailov, S. N.; Vandenoetelaar, L. C. A.; Brongersma, H. H. Strong matrix effect in low-energy He^+ ion-scattering from carbon. *Nucl. Instrum. Methods Phys. Res., Sect. B* **1994**, *93* (2), 210−214. Vandenoetelaar, L. C. A.; Mikhailov, S. N.; Brongersma, H. H. Mechanism of neutralization in Low Energy He^+ Ion Scattering from carbidic and graphitic carbon species on Rhenium. *Nucl. Instrum. Methods Phys. Res., Sect. B* **1994**, *85* (1−4), 420−423.
(35) Jansen, W. P. A.; Knoester, A.; Maas, A. J. H.; Schmit, P.; Kytokivi, A.; Von der Gon, A. W.; Brongersma, H. H. Influence of compaction and surface roughness on low-energy ion scattering signals. *Surf. Interface Anal.* **2004**, *36* (11), 1469−1478.
(36) van den Oetelaar, L. C. A.; van Benthem, H. E.; Helwegen, J.; Stapel, P. J. A.; Brongersma, H. H. Application of low-energy noble-gas ion scattering to the quantitative surface compositional analysis of binary alloys and metal oxides. *Surf. Interface Anal.* **1998**, *26* (8), 537−548.
(37) ter Veen, H. R. J.; Kim, T.; Wachs, I. E.; Brongersma, H. H. Applications of High Sensitivity-Low Energy Ion Scattering (HS-LEIS) in heterogeneous catalysis. *Catal. Today* **2009**, *140* (3−4), 197−201.
(38) Kürnsteiner, P.; Steinberger, R.; Primetzhofer, D.; Goebl, D.; Wagner, T.; Druckmüllerova, Z.; Zeppenfeld, P.; Bauer, P. Matrix effects in the neutralization of He ions at a metal surface containing oxygen. *Surf. Sci.* **2013**, 167−171.
(39) Schmidt, T. J.; Paulus, U. A.; Gasteiger, H. A.; Behm, R. J. The oxygen reduction reaction on a Pt/carbon fuel cell catalyst in the presence of chloride anions. *J. Electroanal. Chem.* **2001**, *508* (1−2), 41−47.

DOI: 10.1021/acs.jpcc.5b02742
J. Phys. Chem. C 2015, 119, 12209−12217